Cooperative Multi-RIS Communications for Wideband mmWave MISO-OFDM Systems

Muxin He, Wei Xu, Hong Shen, Guo Xie, Chunming Zhao, Marco Di Renzo

Cooperative Multi-RIS Communications for Wideband mmWave MISO-OFDM Systems

Muxin He, *Student Member, IEEE*, Wei Xu, *Senior Member, IEEE*, Hong Shen, *Member, IEEE*, Guo Xie, Chunming Zhao, *Member, IEEE*, and Marco Di Renzo, *Fellow, IEEE*

***Abstract*—Reconfigurable intelligent surfaces (RISs) can shape the wireless environment for enhancing the communication performance. In this letter, we propose a cooperative multi-RIS assisted transmission scheme for a millimeter-wave multi-antenna orthogonal frequency division multiplexing system. We first put forward a delay matching based scheme for simultaneously estimating the multipath channels and the transmission delays of distributed RISs, which requires limited training overhead and feedback. Based on this scheme, we obtain a closed-form solution for the RIS phase shift. Then, we derive an analytical expression of the downlink rate, which is proved to increase logarithmically with the square number of RIS reflecting elements. Simulations are conducted to verify these observations.**

***Index Terms*—Channel estimation, millimeter-wave, multiple-input single-output, orthogonal frequency division multiplexing, reconfigurable intelligent surface.**

I. Introduction

In millimeter-wave (mmWave) systems, the signal propagation suffers from severe attenuation and blockages. RISs are, therefore, a promising technology for making mmWave communications more reliable [1]–[5]. In [6], the authors jointly optimized the transmit precoder and the RIS phase shifts in a mmWave system. The impact of hardware impairments on an RIS-assisted system was analyzed in [7]. In [8], an RIS was utilized for improving the channel capacity in a mmWave environment with no line-of-sight (LoS) path. The authors of [9] proposed a stochastic-learning based algorithm for the robust beamforming of an RIS-aided mmWave system.

Most of the currently available research works investigate RIS-assisted systems based on single-carrier modulation [6]–[12]. However, the orthogonal frequency division multiplexing (OFDM) based multi-carrier modulation is commonly used for combatting the frequency-selective fading in wideband systems. Recently, a few studies, e.g., [13]–[15], started investigating multi-carrier RIS-assisted systems, where the same RIS phase shift configuration is assumed across the subcarriers since an RIS cannot provide independent phase control for each subcarrier. To optimize the channel capacity of OFDM systems, the authors of [13] developed an algorithm that yields a locally optimal solution for the joint design of the transmit covariance matrix and the phase shifts of the RIS. In [14], the RIS phase shifts were matched with the phase of the strongest channel path in an OFDM system. In [15], the achievable rate of an OFDM system was maximized by jointly optimizing the power allocation and the RIS phase shifts. A grouping method for the RIS reflecting elements was introduced in [15] to reduce the training overhead. It was shown in [14] and [15] that the large overhead for training and feedback poses a challenge for RIS-aided OFDM communications.

We consider deploying multiple RISs to cooperatively reconfigure the multipath channel for a mmWave multi-antenna OFDM system. Inspired by the method of matching the strongest channel tap in [14], we develop a delay matching based scheme to configure the phases of the distributed RISs based on the transmission delays, which requires low training overhead and limited feedback. The performance enhancement of matching the strongest channel tap is validated by deriving an analytical expression of the downlink rate, which, to the best of our knowledge, has not been provided in the literature. Despite the lack of independent RIS phase control for multiple subcarriers, it is proved that, by using the proposed RIS design, the received power scales with the square of the number of RIS elements even in multi-carrier systems, as previously observed in [6], [7], [16] for single-carrier systems.

II. System Model And Problem Formulation

A. System Model

We consider a multi-RIS aided mmWave multiple-input single-output (MISO)-OFDM system, where a single-antenna UE is served by a base station (BS) and $N_{\rm S}$ RISs. The system can be extended to the multiuser case by using the time division multiple access or the orthogonal frequency division multiple access [17]. $N_{\rm BS}$ antennas are deployed at the BS and M reflecting elements are deployed at each RIS. For mmWave channels with high path loss, the signal reflected by the RIS two or more times is received with negligible power and can be ignored [6], [13], [15], [16]. In the downlink, the signal received, in the frequency domain, at the k-th subcarrier is

$$\begin{aligned} y[k] &= \sqrt{p_{\rm t}}\Big(\sum_{s=0}^{N_{\rm S}-1}(\mathbf{h}_{\rm s}^{\rm r}[k])^H\mathbf{\Theta}_s\mathbf{G}_{\rm s}[k]+(\mathbf{h}^{\rm d}[k])^H\Big)\mathbf{w}[k]s[k]+z[k] \\ &\triangleq \sqrt{p_{\rm t}}\mathbf{h}_{\rm f}^H[k]\mathbf{w}[k]s[k]+z[k], \end{aligned} \tag{1}$$

where $p_{\rm t}$ is the transmit power, $\mathbf{h}_s^{\rm r}[k]\in\mathbb{C}^{M\times 1}$ is the channel from the s-th RIS to the UE, $\mathbf{\Theta}_s\in\mathbb{C}^{M\times M}$ is the diagonal

This work was supported in part by the NSFC under grants 62022026, 61871109, and 61871108, the Natural Science Foundation of Jiangsu Province under Grants BK20190012, BK20201263, and BK20192002, the Shaanxi Key Laboratory of Complex System Control and Intelligent Information Processing (Contract No. 2020CP08), Xi'an University of Technology, China. The work of M. Di Renzo was supported in part by the European Commission through the H2020 ARIADNE project under grant agreement number 871464 and through the H2020 RISE-6G project under grant agreement number 101017011. *(Corresponding authors: Hong Shen; Guo Xie.)*

M. He, W. Xu, H. Shen, and C. Zhao are with the National Mobile Communications Research Laboratory, Southeast University, Nanjing 210096, China (e-mail: mxhe@seu.edu.cn; wxu@seu.edu.cn; shhseu@seu.edu.cn; cmzhao@seu.edu.cn). W. Xu and C. Zhao are also with the Purple Mountain Laboratories, Nanjing 211111, China.

G. Xie is with the Shaanxi Key Laboratory of Complex System Control and Intelligent Information Processing, Xi'an University of Technology, Xi'an 710048, China (e-mail: guoxie@xaut.edu.cn).

M. Di Renzo is with Université Paris-Saclay, CNRS and CentraleSupélec, Laboratoire des Signaux et Systèmes, 91192 Gif-sur-Yvette, France (e-mail: marco.di-renzo@universite-paris-saclay.fr).

matrix of phase shifts of the s-th RIS, $\mathbf{G}_s[k] \in \mathbb{C}^{M\times N_{\rm BS}}$ is the channel from the BS to the s-th RIS, $\mathbf{h}^{\rm d}[k] \in \mathbb{C}^{N_{\rm BS}\times 1}$ is the BS-UE direct channel, $\mathbf{w}[k]\in\mathbb{C}^{N_{\rm BS}\times 1}$ is the BS precoding vector, $s[k]$ is the transmit signal with $\mathbb{E}\{|s[k]|^2\}=1$, $z[k]$ is the additive white Gaussian noise (AWGN) with variance $\sigma_{\rm n}^2$, and $\mathbf{h}_{\rm f}^H[k]$ is the equivalent channel between the BS and the UE. Assuming the presence of few scatterers around high height deployed BS and RISs, the mmWave channel between the BS and each RIS can be assumed to be an LoS channel [6]. We assume that the array response vectors (ARVs) are equal for all the subcarriers as in [18]. Accordingly, we have

$$\mathbf{G}_s[k] = \sqrt{N_{\rm BS}M\beta_s}\eta_s\mathbf{a}_s\mathbf{b}_s^T \triangleq \tilde{\mathbf{G}}_s, \tag{2}$$

where β_s is the large-scale fading factor, η_s is the channel phase, and $\mathbf{a}_s\in\mathbb{C}^{M\times 1}$ and $\mathbf{b}_s\in\mathbb{C}^{N_{\rm BS}\times 1}$ are the ARVs, respectively, of the RIS and the BS, by assuming half-wavelength element spacing. Note that the frequency-domain and the time-domain BS-RIS channels share the same form as in (2) since there exists the LoS path between the BS and each RIS.

In the time domain, a mmWave wideband channel can be expressed as a summation of multiple spatial paths, which are independently reflected by separate scatterers [19]. We assume that the $N_{\rm S}$ RISs are deployed in $N_{\rm S}$ spatially separated locations, which yields the time-domain downlink channel as follows [20]

$$\mathbf{h}^H[n]=\underbrace{\sum_{s=0}^{N_{\rm S}-1}\sum_{l_s=0}^{L_s-1}(\mathbf{h}_{l_s}^{\rm r})^H\mathbf{\Theta}_s\tilde{\mathbf{G}}_s g(nT-\tau_{l_s})}_{\text{reflected channel}}+\underbrace{\sum_{l=0}^{L-1}(\mathbf{h}_l^{\rm d})^H g(nT-\tau_l)}_{\text{direct channel}}, \tag{3}$$

where n is the sampling index, $\mathbf{h}_{l_s}^{\rm r}\in\mathbb{C}^{M\times 1}$ is the l_s-th tap of the channel from the s-th RIS to the UE, which comprises L_s taps, T is the sampling period, τ_{l_s} is the transmission delay of the channel $\mathbf{h}_{l_s}^{\rm r}$, and $g(t)$ is the rectangular pulse shaping filter, i.e., $g(t)=1$ only for $-T\le t<0$ [20]. In the second summation of (3), $\mathbf{h}_l^{\rm d}\in\mathbb{C}^{N_{\rm BS}\times 1}$ is the l-th tap of the BS-UE direct channel, which comprises L taps, and τ_l denotes the corresponding transmission delay. By assuming that the channels are independent and identically distributed and the scatterers are uncorrelated, we have $\mathbf{h}_{l_s}^{\rm r}\sim\mathcal{CN}(\mathbf{0},\beta_s^{\rm r}(\sigma_{l_s}^{\rm r})^2\mathbf{I})$ and $\mathbf{h}_l^{\rm d}\sim\mathcal{CN}(\mathbf{0},\beta\sigma_l^2\mathbf{I})$, where $\beta_s^{\rm r}$ and β are the large-scale fading factors, and $(\sigma_{l_s}^{\rm r})^2$ and σ_l^2 are the normalized small-scale tap powers, i.e., $\sum_{l_s=0}^{L_s-1}(\sigma_{l_s}^{\rm r})^2=1$ and $\sum_{l=0}^{L-1}\sigma_l^2=1$.

Based on (2), it is apparent that the frequency-domain channel $\mathbf{h}_{\rm f}^H[k]$ in (1) and the time-domain channel $\mathbf{h}^H[n]$ in (3) are related via the discrete Fourier transform (DFT):

$$\begin{aligned}\mathbf{h}_{\rm f}^H[k]=&\sum_{s=0}^{N_{\rm S}-1}\sum_{n=0}^{N_{\rm c}-1}\sum_{l_s=0}^{L_s-1}(\mathbf{h}_{l_s}^{\rm r})^H g(nT-\tau_{l_s})e^{-\jmath\frac{2\pi kn}{N_{\rm c}}}\mathbf{\Theta}_s\tilde{\mathbf{G}}_s\\&+\sum_{n=0}^{N_{\rm c}-1}\sum_{l=0}^{L-1}(\mathbf{h}_l^{\rm d})^H g(nT-\tau_l)e^{-\jmath\frac{2\pi kn}{N_{\rm c}}},\end{aligned} \tag{4}$$

where $N_{\rm c}$ is the number of subcarriers.

B. Problem Formulation

Based on the signal model in (1), the downlink rate is

$$\begin{aligned}&R(\mathbf{w}[k],\mathbf{\Theta}_s)\\&=\sum_{k=0}^{N_{\rm c}-1}\log_2\left[1+\frac{p_{\rm t}}{\sigma_{\rm n}^2}\left|\left(\sum_{s=0}^{N_{\rm S}-1}(\mathbf{h}_s^{\rm r}[k])^H\mathbf{\Theta}_s\tilde{\mathbf{G}}_s+(\mathbf{h}^{\rm d}[k])^H\right)\mathbf{w}[k]\right|^2\right].\end{aligned} \tag{5}$$

In order to maximize $R(\mathbf{w}[k],\mathbf{\Theta}_s)$, the joint design of $\mathbf{w}[k]$ and $\mathbf{\Theta}_s$ is formulated as

$$\begin{aligned}\text{P1:}\ \max_{\mathbf{w}[k],\{\mathbf{\Theta}_s\}}\ & R(\mathbf{w}[k],\mathbf{\Theta}_s)\\ \text{s.t.}\ \ & \|\mathbf{w}[k]\|_2^2\le 1,\ k=0,1,...,N_{\rm c}-1\\ & \mathbf{\Theta}_s=\text{diag}\{e^{\jmath\theta_{s,0}},...,e^{\jmath\theta_{s,M-1}}\},\ s=0,1,...,N_{\rm S}-1.\end{aligned} \tag{6}$$

III. Transmission Design

A. Problem Reformulation

For any given $\mathbf{\Theta}_s$ in problem P1, the optimal precoder corresponds to the maximum ratio transmission (MRT) [16]:

$$\mathbf{w}[k]=\frac{\mathbf{h}_{\rm f}[k]}{\|\mathbf{h}_{\rm f}[k]\|_2}=\frac{\sum_{s=0}^{N_{\rm S}-1}\tilde{\mathbf{G}}_s^H\mathbf{\Theta}_s^H\mathbf{h}_s^{\rm r}[k]+\mathbf{h}^{\rm d}[k]}{\left\|\sum_{s=0}^{N_{\rm S}-1}\tilde{\mathbf{G}}_s^H\mathbf{\Theta}_s^H\mathbf{h}_s^{\rm r}[k]+\mathbf{h}^{\rm d}[k]\right\|_2}. \tag{7}$$

Then, by substituting (7) into problem P1, we have

$$\begin{aligned}\max_{\{\mathbf{\Theta}_s\}}\ & \sum_{k=0}^{N_{\rm c}-1}\log_2\left(1+\frac{p_{\rm t}}{\sigma_{\rm n}^2}\left\|\sum_{s=0}^{N_{\rm S}-1}(\mathbf{h}_s^{\rm r}[k])^H\mathbf{\Theta}_s\tilde{\mathbf{G}}_s+(\mathbf{h}^{\rm d}[k])^H\right\|_2^2\right)\\ \text{s.t.}\ \ & \mathbf{\Theta}_s=\text{diag}\{e^{\jmath\theta_{s,0}},...,e^{\jmath\theta_{s,M-1}}\},\ s=0,1,...,N_{\rm S}-1.\end{aligned} \tag{8}$$

Unfortunately, it is difficult to obtain a simple solution to the above problem due to the coupled variables in the objective function. In the following, we provide a low-complexity solution to this problem by transforming the formulation in (8) from the original frequency domain into the time domain.

By applying Jensen's inequality to the rate in (8), we obtain an upper bound of the objective function in problem (8) as

$$\bar{R}=N_{\rm c}\log_2\left[1+\frac{p_{\rm t}}{N_{\rm c}\sigma_{\rm n}^2}\sum_{k=0}^{N_{\rm c}-1}\left\|\sum_{s=0}^{N_{\rm S}-1}(\mathbf{h}_s^{\rm r}[k])^H\mathbf{\Theta}_s\tilde{\mathbf{G}}_s+(\mathbf{h}^{\rm d}[k])^H\right\|_2^2\right]. \tag{9}$$

The bound gets tighter when the channel powers of all subcarriers are more uniform, which corresponds to the considered mmWave band with sparse paths in the time domain. Then, we obtain the channel power maximization problem as

$$\begin{aligned}\text{P2:}\ \max_{\{\mathbf{\Theta}_s\}}\ & \sum_{k=0}^{N_{\rm c}-1}\left\|\sum_{s=0}^{N_{\rm S}-1}(\mathbf{h}_s^{\rm r}[k])^H\mathbf{\Theta}_s\tilde{\mathbf{G}}_s+(\mathbf{h}^{\rm d}[k])^H\right\|_2^2\\ \text{s.t.}\ \ & \mathbf{\Theta}_s=\text{diag}\{e^{\jmath\theta_{s,0}},...,e^{\jmath\theta_{s,M-1}}\},\ s=0,1,...,N_{\rm S}-1.\end{aligned} \tag{10}$$

By applying Parseval's theorem, we recast P2 as

$$\begin{aligned}\max_{\{\mathbf{\Theta}_s\}}\ & \sum_{n=0}^{N_{\rm c}-1}\left\|\sum_{s=0}^{N_{\rm S}-1}\sum_{l_s=0}^{L_s-1}(\mathbf{h}_{l_s}^{\rm r})^H\mathbf{\Theta}_s\tilde{\mathbf{G}}_s g(nT-\tau_{l_s})+\sum_{l=0}^{L-1}(\mathbf{h}_l^{\rm d})^H g(nT-\tau_l)\right\|_2^2\\ \text{s.t.}\ \ & \mathbf{\Theta}_s=\text{diag}\{e^{\jmath\theta_{s,0}},...,e^{\jmath\theta_{s,M-1}}\},\ s=0,1,...,N_{\rm S}-1.\end{aligned} \tag{11}$$

Since $L_s\ll N_{\rm c}$ holds for typical OFDM systems, the channel power is more concentrated in the time domain than in the frequency domain. This is more pronounced in mmWave channels that are characterized by spatial sparsity and severe attenuation. Therefore, we consider matching the RIS phases with the strongest channel tap $\mathbf{h}_{\tilde{l}_s}^{\rm r}$, i.e., the channel tap with the maximum power whose index is denoted by $\tilde{l}_s$. Then, the other

channel taps can be neglected for obtaining a low-complexity solution, which reduces the problem in (11) to

$$\text{P3: } \max_{\{\boldsymbol{\Theta}_s\}} \sum_{s=0}^{N_\mathrm{S}-1} \left\| (\mathbf{h}_{\tilde{l}_s}^{\mathrm{r}})^H \boldsymbol{\Theta}_s \tilde{\mathbf{G}}_s + (\mathbf{h}_{\tilde{l}_s}^{\mathrm{d}})^H \right\|_2^2$$
$$\text{s.t. } \boldsymbol{\Theta}_s = \mathrm{diag}\{e^{\jmath\theta_{s,0}}, ..., e^{\jmath\theta_{s,M-1}}\}, s = 0, 1, ..., N_\mathrm{S}-1,$$

where $\mathbf{h}_{\tilde{l}_s}^{\mathrm{d}}$ is the direct BS-UE channel tap that corresponds to the delay $\tau_{\tilde{l}_s}$. Note that $g(nT-\tau_{\tilde{l}_s})$ is removed in problem P3 since $g(nT-\tau_{\tilde{l}_s}) = 1$ only for $nT < \tau_{\tilde{l}_s} \leq (n+1)T$.

To solve P3, we need the channels $\tilde{\mathbf{G}}_s$, $\mathbf{h}_l^{\mathrm{d}}$, and $\mathbf{h}_{l_s}^{\mathrm{r}}$. Since the positions of the BS and each RIS are fixed, the ARVs $\mathbf{a}_s$, $\mathbf{b}_s$, and the LoS channel $\tilde{\mathbf{G}}_s$ remain static and can be measured after the installation of the RISs [12]. We assume that $\mathbf{h}_{l_s}^{\mathrm{r}}$ can be estimated at the RIS by integrating low-cost receiving circuits into the RIS, as discussed in [1], [2], [5], [16], [21], [22], which can greatly reduce the training overhead of channel estimation compared to a passive RIS. Since low-complexity RISs are more vulnerable to channel estimation errors, we focus on the estimation of $\mathbf{h}_{l_s}^{\mathrm{r}}$ at each RIS while assume that $\mathbf{h}_l^{\mathrm{d}}$ is perfectly obtained at the BS. Note that the signal reflected by RIS undergoes a different transmission delay. Hence, we need to perform the delay matching and the phase design for each RIS individually.

B. Channel Estimation and RIS Delay Matching

As for the estimation of the uplink UE-RIS channel at each RIS, the UE first transmits a pilot signal $\mathbf{x} \in \mathbb{C}^{N_\mathrm{c} \times 1}$. Then, the received frequency-domain signal at the i-th reflecting element of the s-th RIS is

$$\mathbf{y}_s^{\mathrm{r},i} = \sqrt{p_\mathrm{p} N_\mathrm{c}} \boldsymbol{\Phi} \mathbf{F}_{L_s} \mathbf{h}_s^{\mathrm{r},i} + \mathbf{z}_s^{\mathrm{r}} \triangleq \mathbf{A}_s^{\mathrm{r}} \mathbf{h}_s^{\mathrm{r},i} + \mathbf{z}_s^{\mathrm{r}}, \tag{12}$$

where p_p is the transmit power at the UE, $\boldsymbol{\Phi} \triangleq \mathrm{diag}\{\mathbf{x}\}$, $\mathbf{F}_{L_s}$ comprises the first L_s columns of the DFT matrix $\mathbf{F}$, $\mathbf{h}_s^{\mathrm{r},i} \in \mathbb{C}^{L_s \times 1}$ is the multipath channel at the i-th reflecting element of the RIS, $\mathbf{z}_s^{\mathrm{r}} \sim \mathcal{CN}(\mathbf{0}, \sigma_z^2 \mathbf{I})$ denotes the AWGN. From (12), the time-domain channel $\mathbf{h}_s^{\mathrm{r},i}$ can be estimated by using the linear minimum mean squared error method as

$$\hat{\mathbf{h}}_s^{\mathrm{r},i} = \mathbf{R}_s \left[(\mathbf{A}_s^{\mathrm{r}})^H \mathbf{A}_s^{\mathrm{r}} \mathbf{R}_s + \sigma_z^2 \mathbf{I} \right]^{-1} (\mathbf{A}_s^{\mathrm{r}})^H \mathbf{y}_s^{\mathrm{r},i}, \tag{13}$$

where $\mathbf{R}_s$ is the autocorrelation matrix of $\mathbf{h}_s^{\mathrm{r},i}$. We define the estimation error by $\mathbf{e}_s^{\mathrm{r},i} = \mathbf{h}_s^{\mathrm{r},i} - \hat{\mathbf{h}}_s^{\mathrm{r},i}$, and have

$$\mathbb{E}\left[\mathbf{e}_s^{\mathrm{r},i} (\mathbf{e}_s^{\mathrm{r},i})^H \right] = \sigma_z^2 \mathbf{R}_s \left[(\mathbf{A}_s^{\mathrm{r}})^H \mathbf{A}_s^{\mathrm{r}} \mathbf{R}_s + \sigma_z^2 \mathbf{I} \right]^{-1}. \tag{14}$$

Therefore, the desired channel estimate $\hat{\mathbf{h}}_{l_s}^{\mathrm{r}}$ is the l_s-th column of the matrix $[\hat{\mathbf{h}}_s^{\mathrm{r},0}, \hat{\mathbf{h}}_s^{\mathrm{r},1}, ..., \hat{\mathbf{h}}_s^{\mathrm{r},M-1}]^T$. The UE-BS direct channel is obtained by the BS at the same time.

Since $\hat{\mathbf{h}}_{l_s}^{\mathrm{r}}$ and $\mathbf{h}_l^{\mathrm{d}}$ are obtained at different terminals, the corresponding delays are, in general not aligned, and, therefore, need to be matched for solving P3. In other words, it is necessary to determine the right tap in $\mathbf{h}_l^{\mathrm{d}}$ that corresponds to $\hat{\mathbf{h}}_{l_s}^{\mathrm{r}}$. To achieve this goal, we first match the RIS phase shifts to the strongest path of the UE-RIS-BS channel, which amounts to maximizing the power of the cascaded channel $\tilde{\mathbf{G}}_s^H \boldsymbol{\Theta}_s^H \hat{\mathbf{h}}_{\tilde{l}_s}^{\mathrm{r}}$. To this end, it can be readily verified that the RIS phase matrix needs to be set to

$$\boldsymbol{\Theta}_s^{\mathrm{p}} = \mathrm{diag}\left\{ e^{-\jmath \mathrm{arg}[\eta_s (\hat{\mathbf{h}}_{\tilde{l}_s}^{\mathrm{r}})^* \circ \mathbf{a}_s]} \right\}, \tag{15}$$

where $(\cdot)^*$ is the conjugate operation and $\circ$ is the Hadamard product [6]. Then, by subtracting the UE-BS direct channel from the overall UE-BS channel, we obtain the time-domain UE-RIS-BS cascaded channel at the BS as follows:

$$\mathbf{h}_\mathrm{s}[n] = \sum_{s=0}^{N_\mathrm{S}-1} \tilde{\mathbf{G}}_s^H (\boldsymbol{\Theta}_s^{\mathrm{p}})^H \sum_{l_s=0}^{L_s-1} \mathbf{h}_{l_s}^{\mathrm{r}} g(nT - \tau_{l_s}). \tag{16}$$

To match the delay of $\mathbf{h}_{l_j}^{\mathrm{r}}$ and $\mathbf{h}_l^{\mathrm{d}}$, we multiply the sequence $\mathbf{h}_\mathrm{s}[n]$ with $\mathbf{b}_j^T$, and obtain

$$\begin{aligned} h_j[n] &= \mathbf{b}_j^T \mathbf{h}_\mathrm{s}[n] = \sqrt{N_\mathrm{BS} \beta_j} \left\| \hat{\mathbf{h}}_{\tilde{l}_j}^{\mathrm{r}} \right\|_1 g(nT - \tau_{\tilde{l}_j}) \\ &+ \sqrt{N_\mathrm{BS} M \beta_j} \eta_j^* \mathbf{a}_j^H (\boldsymbol{\Theta}_j^{\mathrm{p}})^H \sum_{\{l_j\} \backslash \{\tilde{l}_j\}} \mathbf{h}_{l_j}^{\mathrm{r}} g(nT - \tau_{l_j}) \\ &+ \sum_{\{s\} \backslash \{j\}} \sqrt{N_\mathrm{BS} M \beta_s} \eta_s^* \mathbf{b}_j^T \mathbf{b}_s^* \mathbf{a}_s^H (\boldsymbol{\Theta}_s^{\mathrm{p}})^H \sum_{l_s=0}^{L_s-1} \mathbf{h}_{l_s}^{\mathrm{r}} g(nT - \tau_{l_s}), \end{aligned} \tag{17}$$

where $\|\cdot\|_1$ denotes the 1-norm of a vector, $\{l_j\} \backslash \{\tilde{l}_j\}$ denotes the set of taps excluding the strongest tap $\tilde{l}_j$, and $\{s\} \backslash \{j\}$ denotes the set of RISs excluding the j-th RIS. According to (17), the CSI of the j-th RIS is extracted from $\mathbf{h}_\mathrm{s}[n]$ due to the fact that $\mathbf{b}_j^T \mathbf{b}_s^* \to 0$ $(j \neq s)$ as $N_\mathrm{BS} \to \infty$, which makes the third term in (17) to vanish. Moreover, by using $\boldsymbol{\Theta}_j^{\mathrm{p}}$ in (15), the first term of (17) is dominant. Therefore, the tap index of $\mathbf{h}_{l_j}^{\mathrm{r}}$, i.e., $\tilde{l}_j$, can be obtained at the BS by selecting the tap that corresponds to the maximum power in (17). Then, the corresponding tap of the UE-BS direct channel, i.e., $\mathbf{h}_{\tilde{l}_j}^{\mathrm{d}}$, is employed in P3 for designing the phases of the j-th RIS.

C. Phase Design for Multiple RISs

With the delay matched at the BS and $\hat{\mathbf{h}}_{\tilde{l}_s}^{\mathrm{r}}$, P3 can be decoupled into N_S subproblems, where each subproblem is

$$\text{P4: } \max_{\boldsymbol{\Theta}_s} \left\| (\hat{\mathbf{h}}_{\tilde{l}_s}^{\mathrm{r}})^H \boldsymbol{\Theta}_s \tilde{\mathbf{G}}_s + (\mathbf{h}_{\tilde{l}_s}^{\mathrm{d}})^H \right\|_2^2 \tag{18}$$
$$\text{s.t. } \boldsymbol{\Theta}_s = \mathrm{diag}\{e^{\jmath\theta_{s,0}}, e^{\jmath\theta_{s,1}}, ..., e^{\jmath\theta_{s,M-1}}\}.$$

This problem admits a closed-form solution as follows [6]

$$\bar{\boldsymbol{\Theta}}_s = e^{\jmath\alpha_s} \mathrm{diag}\left\{ e^{-\jmath \mathrm{arg}\left[\eta_s (\hat{\mathbf{h}}_{\tilde{l}_s}^{\mathrm{r}})^* \circ \mathbf{a}_s\right]} \right\}, \tag{19}$$

where $\alpha_s = -\mathrm{arg}\{\mathbf{b}_s^T \mathbf{h}_{\tilde{l}_s}^{\mathrm{d}}\}$ is calculated at the BS using the matched delay, and $\mathrm{arg}[\cdot]$ denotes the angle of the input. It can be readily verified that (19) is also optimal for P3. Note that the RIS phase shift design in (19) aligns the reflected signal to the strongest channel tap between the RIS and the UE.

Remark 1: The closed-form solution in (19) accounts for the impact of multi-carrier modulation and channel estimation, which encompasses the case study of single-carrier modulation under perfect CSI considered in [6] as a special case.

Remark 2: It is observed from (19) that α_s and $\hat{\mathbf{h}}_{\tilde{l}_s}^{\mathrm{r}}$ need to be known at each RIS in order to perform phase matching. Since both the estimate and the phase matching of the high-dimensional channel $\hat{\mathbf{h}}_{\tilde{l}_s}^{\mathrm{r}}$ are obtained locally at each RIS, the BS only needs to transmit one scalar α_s to the corresponding RIS without feeding back the high-dimensional phase matrix. Moreover, during the channel training, each RIS only needs to reset the phase matrix twice, respectively in (15) and (19), which also reduces the control overhead.

IV. Performance Analysis

Theorem 1: Given the imperfect CSI at multiple RISs and the phase matrix $\bar{\boldsymbol{\Theta}}_s$ in (19), by assuming multipath Rician fading for each BS-RIS channel with a K-factor K_G, the downlink achievable rate can be approximated, in a closed-form expression, as

$$\mathbb{E}[\bar{R}] \approx N_{\mathrm{c}} \log_2 \left\{ 1 + \frac{p_{\mathrm{t}}}{N_{\mathrm{c}} \sigma_{\mathrm{n}}^2} \left[\sum_{s=0}^{N_{\mathrm{S}}-1} \frac{K_G M (M-1) N_{\mathrm{BS}} \beta_s \beta_s^{\mathrm{r}} \pi (\hat{\sigma}_{\tilde{l}_s}^{\mathrm{r}})^2}{4(K_G+1)} + \sqrt{\frac{K_G N_{\mathrm{BS}} \beta_s \beta_s^{\mathrm{r}} \beta}{K_G+1}} \frac{M \pi \hat{\sigma}_{\tilde{l}_s}^{\mathrm{r}} \sigma_{\tilde{l}_s}}{2} + M N_{\mathrm{BS}} \beta_s \beta_s^{\mathrm{r}} + N_{\mathrm{BS}} \beta \right] \right\}, \quad (20)$$

where $(\hat{\sigma}_{\tilde{l}_s}^{\mathrm{r}})^2 = p_{\mathrm{p}} N_{\mathrm{c}} \beta_s^{\mathrm{r}} (\sigma_{\tilde{l}_s}^{\mathrm{r}})^4 / [p_{\mathrm{p}} N_{\mathrm{c}} \beta_s^{\mathrm{r}} (\sigma_{\tilde{l}_s}^{\mathrm{r}})^2 + \sigma_z^2]$.

Proof: See Appendix A. ∎

Remark 3: In contrast with the design of RISs in single-carrier systems, matching the phase of the strongest channel tap in multi-carrier systems results in a mismatch for the phases of the other taps, i.e., $\mathbf{h}_{l_s}^{\mathrm{r}}$ $(l_s \neq \tilde{l}_s)$. Fortunately, the power of the mismatched channel tap derived in (24) reveals that there is no loss in the average power since the mismatched phase shifts provide the same average power as the non-optimized case with random phase shifts. Therefore, matching the phase of the strongest channel tap under multipath channels ensures that a non-zero power increment $\Delta\gamma_s$, which is derived in Appendix A in (25), can be obtained from each RIS.

Remark 4: Although the closed-form design in (19) is derived for a multi-carrier system under imperfect CSI, it yields the same scaling law as the special case of single-carrier systems under perfect CSI, e.g., [6], [7], [16]. Concretely, when $M \to \infty$, the derived results of the average channel power in (23) and the downlink rate in (20) increase linearly and logarithmically with the square number of RIS reflecting elements, respectively.

V. Numerical Results

We assume that the BS with $N_{\mathrm{BS}} = 32$ antennas is at the origin point, the UE is at $(40, 0)$ m, and $N_{\mathrm{S}} = 3$ RISs are at $(20, 20\tan\phi_s)$ m, where $\phi_0 = -\pi/6$, $\phi_1 = \pi/8$, $\phi_2 = \pi/4$ are the angles of departure of each BS-RIS channel. We define the path loss as $\mathrm{PL} \triangleq \mathrm{PL}_0 + 10\zeta \log_{10}(d)$, where $\mathrm{PL}_0 = 30$ dB is the path loss at the reference distance of 1 m, ζ is the path loss exponent (PLE), and d is the distance. Then, the large-scale fading factor $\beta = 10^{-0.1\mathrm{PL}}$. The PLEs of $\mathbf{h}_s^{\mathrm{r}}$, $\tilde{\mathbf{G}}_s$, and $\mathbf{h}^{\mathrm{d}}$ are 2.2, 2.5, and 3.5, respectively. The transmit powers of the BS and the UE are $p_{\mathrm{t}} = 10$ dBm and $p_{\mathrm{p}} = 0$ dBm, respectively, and the noise power of the UE is $\sigma_{\mathrm{n}}^2 = -100$ dBm. The normalized profiles of $\mathbf{h}_s^{\mathrm{r}}$ and $\mathbf{h}^{\mathrm{d}}$ are assumed to be linear descending with an attenuation step of -3 dB between adjacent taps. Uniform profiles with two taps are assumed for the non-LoS BS-RIS channels. The number of taps of each RIS-UE channel are $L_0 = L_1 = 3$ and $L_2 = 2$. The transmission delay is calculated by dividing the distance between the communication nodes by the speed of light, and the delay of one tap is 10 ns. The rectangular pulse shaping filter is used. The number of subcarriers is $N_{\mathrm{c}} = 64$ and the length of the OFDM cyclic prefix (CP) is $L_{\mathrm{CP}} = 8$. In a transmission frame, the first three symbols are used for the channel estimation at the RISs, the delay matching at BS, and the estimation of the equivalent BS-UE channel $\mathbf{h}_{\mathrm{f}}[k]$ that is needed for MRT precoding, respectively. On the other hand, the remaining symbols are used for downlink data transmission.

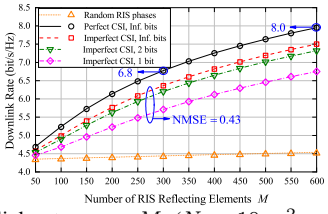

Fig. 1. The downlink rate versus M. ($N_{\mathrm{T}} = 10$, $\sigma_z^2 = -50$ dBm)

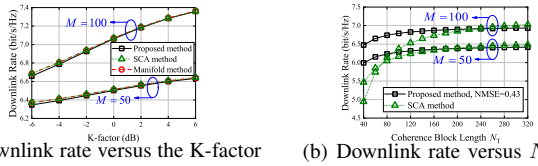

(a) Downlink rate versus the K-factor (b) Downlink rate versus N_{T}

Fig. 2. The downlink rate of different transmission methods.

Fig. 1 displays the downlink rate with respect to M. The coherence block length is $N_{\mathrm{T}} = 10$ OFDM symbols, and the K-factor of the BS-RIS channel is 5 dB. The noise power at the RISs $\sigma_z^2 = -50$ dBm which corresponds to a normalized mean squared error (NMSE) of 0.43. For the first three curves, the markers and the lines correspond to the numerical results and the analytical results in (20), respectively. The numerical results are averaged over 500 channel realizations by using the exact expression of the instantaneous rate, where the proposed delay matching method is applied. It is found that the analytical results match the numerical results well. By using the closed-form RIS design in (19), the rate increases logarithmically with M^2 when M is large. Specially, from $M = 300$ to $M = 600$, the rate increases by 1.2 bit/s/Hz $\approx \frac{N_{\mathrm{c}}}{N_{\mathrm{c}}+L_{\mathrm{CP}}} \frac{N_{\mathrm{T}}-3}{N_{\mathrm{T}}} \log_2(4)$. We also simulate the performance when quantizing the RIS phase shifts with 1-bit and 2-bit in Fig. 1. The rate of 2-bit RIS phase shifts approaches the rate without using quantization. Furthermore, we compare the proposed method with the successive convex approximation (SCA) method [15] and the manifold method [23], which consider all the channel taps. In Fig. 2 (a), the performance of the proposed method approaches that of the SCA method and the manifold method, even when the K-factor of the BS-RIS channel is small. In Fig. 2 (b), we simulate the downlink rate that considers the impact of training overhead, where the SCA based method in [15] with a grouping ratio of $1/25$ is adopted as the benchmark scheme. It is found that the proposed method can achieve a higher rate for relatively short coherence block lengths N_{T}, thanks to the reduced training overhead.

VI. Conclusion

We proposed a delay matching based scheme to decouple the cooperative multi-RIS design in a mmWave MISO-OFDM system, which results in a reduced overhead and limited feedback. Despite the lack of independent RIS phase control for multiple subcarriers, the proposed RIS design was proved to provide the square scaling law for OFDM systems as well. Future works include the extension of this work to space division multiple access (SDMA) based multiuser systems.

APPENDIX A
PROOF OF THEOREM 1

By using pilots of constant modulus, i.e., $\mathbf{\Phi}^H\mathbf{\Phi}=\mathbf{I}$, in (12) and (13), the autocorrelation matrix of $\hat{\mathbf{h}}_s^{\mathrm{r},i}$ is a diagonal matrix. Each entry of $\hat{\mathbf{h}}_{l_s}^{\mathrm{r}}$ has variance equal to

$$\mathbb{V}[\hat{h}_{l_s}^{\mathrm{r}}]=\mathbb{V}[h_{l_s}^{\mathrm{r}}]-\sigma_{el_s}^2=\frac{p_{\mathrm{p}}N_{\mathrm{c}}(\beta_s^{\mathrm{r}})^2(\sigma_{l_s}^{\mathrm{r}})^4}{p_{\mathrm{p}}N_{\mathrm{c}}\beta_s^{\mathrm{r}}(\sigma_{l_s}^{\mathrm{r}})^2+\sigma_z^2}\triangleq\beta_s^{\mathrm{r}}(\hat{\sigma}_{l_s}^{\mathrm{r}})^2, \quad (21)$$

where $\sigma_{el_s}^2$ is the estimation error variance of $h_{l_s}^{\mathrm{r}}$ based on (14). Therefore, $\hat{\mathbf{h}}_{l_s}^{\mathrm{r}}\sim\mathcal{CN}(\mathbf{0},\beta_s^{\mathrm{r}}(\hat{\sigma}_{l_s}^{\mathrm{r}})^2\mathbf{I})$.

By using [24, Lemma 1] and Parseval's theorem, we approximate the expectation of (9) as

$$\mathbb{E}[\bar{R}]\approx N_{\mathrm{c}}\log_2\left(1+\frac{p_{\mathrm{t}}}{N_{\mathrm{c}}\sigma_{\mathrm{n}}^2}\mathbb{E}\left[\sum_{n=0}^{N_{\mathrm{c}}-1}\|\mathbf{h}[n]\|_2^2\right]\right), \quad (22)$$

which is tighter as the number of BS antennas increases [24]. We replace the simplified LoS BS-RIS channel $\tilde{\mathbf{G}}_s$ in (3) by a multipath Rician channel $\bar{\mathbf{G}}_s=[\bar{\mathbf{G}}_{s,0}g(nT-\tau_0),...,\bar{\mathbf{G}}_{s,L_G}g(nT-\tau_{L_G})]$ with L_G+1 taps, where $\bar{\mathbf{G}}_{s,0}=\sqrt{K_G/(K_G+1)}\tilde{\mathbf{G}}_s$ is the LoS tap and $\bar{\mathbf{G}}_{s,l_G}$ $(l_G>0)$ follows $\mathcal{CN}(0,\beta_s\sigma_{l_G}^2/(K_G+1))$ with $\sum_{l_G=1}^{L_G}\sigma_{l_G}^2=1$. Then, we can rewrite each BS-RIS-UE channel in (3) as $(\mathbf{h}_s^{\mathrm{r}})^H\star\bar{\mathbf{\Theta}}_s\star\bar{\mathbf{G}}_s$, where $(\mathbf{h}_s^{\mathrm{r}})^H=\sum_{l_s=0}^{L_s-1}(\mathbf{h}_{l_s}^{\mathrm{r}})^Hg(nT-\tau_{l_s})$ and $\star$ denotes the convolution operation.

By using the RIS phases in (19), $\mathbf{h}_{\tilde{l}_s}^{\mathrm{r}}=\hat{\mathbf{h}}_{\tilde{l}_s}^{\mathrm{r}}+\mathbf{e}_{\tilde{l}_s}$, and the fact that $\hat{\mathbf{h}}_{\tilde{l}_s}^{\mathrm{r}}$, $\mathbf{e}_{\tilde{l}_s}$, and $\mathbf{h}_{\tilde{l}_s}^{\mathrm{d}}$ are independent, the power of the tap that corresponds to $(\mathbf{h}_{\tilde{l}_s}^{\mathrm{r}})^H\bar{\mathbf{\Theta}}_s\bar{\mathbf{G}}_{s,0}$ is calculated as

$$\begin{aligned}\bar{\gamma}_{\tilde{l}_s}&\triangleq\mathbb{E}\left[\left\|(\mathbf{h}_{\tilde{l}_s}^{\mathrm{r}})^H\bar{\mathbf{\Theta}}_s\bar{\mathbf{G}}_{s,0}+(\mathbf{h}_{\tilde{l}_s}^{\mathrm{d}})^H\right\|_2^2\right]\\&=\frac{K_GM(M-1)N_{\mathrm{BS}}\beta_s\beta_s^{\mathrm{r}}\pi(\hat{\sigma}_{\tilde{l}_s}^{\mathrm{r}})^2}{4(K_G+1)}+\frac{K_GMN_{\mathrm{BS}}\beta_s\beta_s^{\mathrm{r}}(\sigma_{\tilde{l}_s}^{\mathrm{r}})^2}{K_G+1}\\&\quad+\sqrt{\frac{K_GN_{\mathrm{BS}}\beta_s\beta_s^{\mathrm{r}}\beta}{K_G+1}}\frac{M\pi\hat{\sigma}_{\tilde{l}_s}^{\mathrm{r}}\sigma_{\tilde{l}_s}}{2}+N_{\mathrm{BS}}\beta\sigma_{\tilde{l}_s}^2. \quad (23)\end{aligned}$$

For any tap corresponding to $(\mathbf{h}_{l_s}^{\mathrm{r}})^H\bar{\mathbf{\Theta}}_s\bar{\mathbf{G}}_{s,l_G}(l_s\neq\tilde{l}_s$ or $l_G\neq0)$ that is not aligned by $\bar{\mathbf{\Theta}}_s$ in (19), the tap power is

$$\gamma_{l_s}^{\mathrm{mis}}=c_{l_G}MN_{\mathrm{BS}}\beta_s\beta_s^{\mathrm{r}}(\sigma_{l_s}^{\mathrm{r}})^2+N_{\mathrm{BS}}\beta\sigma_l^2=\gamma_{l_s}^{\mathrm{ran}}, \quad (24)$$

where $c_{l_G}=K_G/(K_G+1)$ for $l_G=0$, $c_{l_G}=\sigma_{l_G}^2/(K_G+1)$ for $l_G\neq0$, and $\gamma_{l_s}^{\mathrm{ran}}$ is the tap power with random RIS phase shifts. Then, the power increment provided by the s-th RIS is

$$\begin{aligned}\Delta\gamma_s&=\bar{\gamma}_{\tilde{l}_s}-\gamma_{\tilde{l}_s}^{\mathrm{ran}}\\&=\frac{K_GM(M-1)N_{\mathrm{BS}}\beta_s\beta_s^{\mathrm{r}}\pi(\hat{\sigma}_{\tilde{l}_s}^{\mathrm{r}})^2}{4(K_G+1)}+\sqrt{\frac{K_GN_{\mathrm{BS}}\beta_s\beta_s^{\mathrm{r}}\beta}{K_G+1}}\frac{M\pi\hat{\sigma}_{\tilde{l}_s}^{\mathrm{r}}\sigma_{\tilde{l}_s}}{2}. \quad (25)\end{aligned}$$

The total channel power based on random RIS phase shifts is

$$\gamma^{\mathrm{ran}}=\sum_{s=0}^{N_{\mathrm{S}}-1}MN_{\mathrm{BS}}\beta_s\beta_s^{\mathrm{r}}+N_{\mathrm{BS}}\beta. \quad (26)$$

Therefore, we use the term γ^{ran} in (26) and the increment term $\Delta\gamma_s$ in (25) to derive (22) as

$$\mathbb{E}[\bar{R}]\approx N_{\mathrm{c}}\log_2\left(1+\frac{p_{\mathrm{t}}}{N_{\mathrm{c}}\sigma_{\mathrm{n}}^2}\left[\gamma^{\mathrm{ran}}+\sum_{s=0}^{N_{\mathrm{S}}-1}\Delta\gamma_s\right]\right), \quad (27)$$

from which we obtain (20).

REFERENCES

[1] Q. Wu and R. Zhang, "Towards smart and reconfigurable environment: Intelligent reflecting surface aided wireless network," *IEEE Commun. Mag.*, vol. 58, no. 1, pp. 106–112, Jan. 2020.

[2] M. Di Renzo *et al.*, "Smart radio environments empowered by reconfigurable AI meta-surfaces: An idea whose time has come," *EURASIP J. Wireless Commun. Netw.*, vol. 2019, no. 1, pp. 1–20, May 2019.

[3] E. Basar *et al.*, "Wireless communications through reconfigurable intelligent surfaces," *IEEE Access*, vol. 7, pp. 116 753–116 773, Aug. 2019.

[4] M. Di Renzo *et al.*, "Reconfigurable intelligent surfaces vs. relaying: Differences, similarities, and performance comparison," *IEEE Open J. Commun. Soc.*, vol. 1, pp. 798–807, Jun. 2020.

[5] ——, "Smart radio environments empowered by reconfigurable intelligent surfaces: How it works, state of research, and the road ahead," *IEEE J. Sel. Areas Commun.*, vol. 38, no. 11, pp. 2450–2525, Nov. 2020.

[6] P. Wang *et al.*, "Intelligent reflecting surface-assisted millimeter wave communications: Joint active and passive precoding design," *IEEE Trans. Veh. Technol.*, vol. 69, no. 12, pp. 14 960–14 973, Dec. 2020.

[7] S. Zhou *et al.*, "Spectral and energy efficiency of IRS-assisted MISO communication with hardware impairments," *IEEE Wireless Commun. Lett.*, vol. 9, no. 9, pp. 1366–1369, Sep. 2020.

[8] N. S. Perović *et al.*, "Channel capacity optimization using reconfigurable intelligent surfaces in indoor mmwave environments," in *Proc. IEEE ICC*, Dublin, Ireland, Jun. 2020, pp. 1–7.

[9] G. Zhou *et al.*, "Stochastic learning-based robust beamforming design for RIS-aided millimeter-wave systems in the presence of random blockages," *IEEE Trans. Veh. Technol.*, vol. 70, no. 1, pp. 1057–1061, Jan. 2021.

[10] H. Shen *et al.*, "Secrecy rate maximization for intelligent reflecting surface assisted multi-antenna communications," *IEEE Commun. Lett.*, vol. 23, no. 9, pp. 1488–1492, Sep. 2019.

[11] H. Shen *et al.*, "Beamformig design with fast convergence for IRS-aided full-duplex communication," *IEEE Commun. Lett.*, vol. 24, no. 12, pp. 2849–2853, Dec. 2020.

[12] Y. Han *et al.*, "Large intelligent surface-assisted wireless communication exploiting statistical CSI," *IEEE Trans. Veh. Technol.*, vol. 68, no. 8, pp. 8238–8242, Aug. 2019.

[13] S. Zhang and R. Zhang, "Capacity characterization for intelligent reflecting surface aided MIMO communication," *IEEE J. Sel. Areas Commun.*, vol. 38, no. 8, pp. 1823–1838, Aug. 2020.

[14] B. Zheng and R. Zhang, "Intelligent reflecting surface-enhanced OFDM: Channel estimation and reflection optimization," *IEEE Wireless Commun. Lett.*, vol. 9, no. 4, pp. 518–522, Apr. 2019.

[15] Y. Yang *et al.*, "Intelligent reflecting surface meets OFDM: Protocol design and rate maximization," *IEEE Trans. Commun.*, vol. 68, no. 7, pp. 4522–4535, Jul. 2020.

[16] Q. Wu and R. Zhang, "Intelligent reflecting surface enhanced wireless network via joint active and passive beamforming," *IEEE Trans. Wireless Commun.*, vol. 18, no. 11, pp. 5394–5409, Nov. 2019.

[17] B. Zheng *et al.*, "Intelligent reflecting surface assisted multi-user OFDMA: Channel estimation and training design," *IEEE Trans. Wireless Commun.*, vol. 19, no. 12, pp. 8315–8329, Dec. 2020.

[18] F. Sohrabi and W. Yu, "Hybrid analog and digital beamforming for mmWave OFDM large-scale antenna arrays," *IEEE J. Sel. Areas Commun.*, vol. 35, no. 7, pp. 1432–1443, Jul. 2017.

[19] M. Stege *et al.*, "A multiple input-multiple output channel model for simulation of Tx-and Rx-diversity wireless systems," in *Proc. IEEE VTC*, Boston, MA, Sep. 2000, pp. 833–839.

[20] J. Du *et al.*, "Weighted spectral efficiency optimization for hybrid beamforming in multiuser massive MIMO-OFDM systems," *IEEE Trans. Veh. Technol.*, vol. 68, no. 10, pp. 9698–9712, Oct. 2019.

[21] G. C. Alexandropoulos and E. Vlachos, "A hardware architecture for reconfigurable intelligent surfaces with minimal active elements for explicit channel estimation," in *Proc. IEEE ICASSP*, Barcelona, Spain, May 2020, pp. 9175–9179.

[22] A. Taha *et al.*, "Enabling large intelligent surfaces with compressive sensing and deep learning," *IEEE Access*, vol. 9, pp. 44 304–44 321, 2021.

[23] X. Yu *et al.*, "MISO wireless communication systems via intelligent reflecting surfaces: (invited paper)," in *Proc. IEEE/CIC ICCC*, Changchun, China, Aug. 2019, pp. 735–740.

[24] Q. Zhang *et al.*, "Power scaling of uplink massive MIMO systems with arbitrary-rank channel means," *IEEE J. Sel. Topics Signal Process.*, vol. 8, no. 5, pp. 966–981, Oct. 2014.